

Minimizing electro-optical losses of ITO layers for monolithic perovskite silicon tandem solar cells

Özde Ş. Kabaklı^{a,*}, Jakob Kox^a, Leonard Tutsch^a, Minasadat Heydarian^{a,b}, Alexander J. Bett^a, Stefan Lange^c, Oliver Fischer^{a,b}, Christian Hagendorf^c, Martin Bivour^a, Martin Hermle^a, Patricia S.C. Schulze^a, Jan Christoph Goldschmidt^{a,d}

^a Fraunhofer Institute for Solar Energy Systems, Heidenhofstrasse 2, 79110, Freiburg, Germany

^b University of Freiburg, Department of Sustainable Systems Engineering INATECH, Emmy-Noether-Straße 2, 79108, Freiburg Im Breisgau, Germany

^c Fraunhofer Center for Silicon-Photovoltaics, Otto-Eißfeldt-Straße 12, 06120, Halle, Saale, Germany

^d University of Marburg, Department of Physics, Biegenstraße 10, 35037, Marburg, Germany

ABSTRACT

Monolithic perovskite silicon tandem solar cells promise high efficiency and cost advantage. In such tandem devices a conductive front electrode of high transparency is necessary for lateral transportation of the charges.

This study focuses on optimizing the electro-optical properties of DC sputtered ITO films as front electrode in monolithic two-terminal perovskite silicon tandem solar cells. Initially, an ITO thin film is developed by finding a possible optimum doping level that provides both high transparency and low sheet resistance. Moreover, to further decouple the transparency-conductivity trade-off of the ITO bulk properties from the requirements for low-ohmic contact formation, a thin, highly doped ITO interlayer is inserted towards the SnO_x interface. The ITO thin film (stack) significantly improved efficiency of the tandem solar cells by improving all solar cell parameters. This optimization led to improved tandem short circuit density with reduced standard deviation from a mean value of $19.3 \pm 0.4 \text{ mA/cm}^2$ to $19.8 \pm 0.2 \text{ mA/cm}^2$, increased average fill factor from 68% to 73% and average power conversion efficiency increase from 22% to 25%.

1. Introduction

Silicon solar cells are approaching their theoretical efficiency limit of 29.4% [1,2]. Tandem solar cells promise reaching higher efficiencies by utilizing the solar spectrum more efficiently. Perovskite solar cells are promising candidates for coupling with silicon in tandem structure as a top solar cell. Organic-inorganic lead halides are especially promising due to facile processing, abundant availability of the raw materials, exceptional electro-optical properties, adjustable bandgap and high defect tolerance [3–7]. A 2-terminal monolithic tandem configuration is advantageous for module integration since it eliminates the need for rear and front electrodes for the top and bottom cell respectively. 2-terminal perovskite silicon tandem solar cells in lab scale have already reached 31.3% power conversion efficiency, in line with the optical simulation results and ensuring the potential of the perovskite silicon tandem solar cell technology [2,8,9].

Effective light management in the tandem solar cell stack is necessary to reduce the optical losses and maximize the absorption in the absorber layers [10]. Transparent and conductive electrodes are one of the necessary layers for realizing monolithic perovskite silicon tandem

solar cells. Transparent conductive oxides (TCOs) offer good electro-optical properties with facile processing and are used widely among other transparent and conductive electrodes [11]. One of the most used TCOs is indium tin oxide (ITO) due to its superior electro-optical properties and stability. Among various applications, the commonly used ITO composition is 90 wt% In₂O₃ and 10 wt% SnO₂ [10, 12]. Typically sputtering is applied as deposition method for TCOs and is available for industrial scale applications. However, detailed optimization of the sputter process is necessary since the unwanted optical properties correlate with wanted electrical properties, such as increasing parasitic absorption with increasing free carrier density. Moreover, direct sputtering of TCOs on perovskite top solar cells is challenging due to the risk of damaging the organic layers and the perovskite layer underneath by altering their chemical bonding [13–15]. Introducing a buffer layer under the TCO, such as SnO_x deposited via ALD in the p-i-n perovskite solar cell stack, is a common method of mitigating the risk of sputter damage [16–20].

In this work, the development of an electro-optically optimized ITO thin film with low sheet resistance and low absorptance as well as an ITO stack film with further improved contact to the SnO_x buffer layer are

* Corresponding author.

E-mail address: oezde.seyma.kabakli@ise.fraunhofer.de (Ö.Ş. Kabaklı).

presented. The optimized films are implemented into perovskite silicon tandem solar cells. The low sheet resistance and absorptance are achieved by fine-tuning the oxygen flow rate during the sputtering process of the ITO films.

2. Results

A low damage ITO sputter process using a 90 wt% In_2O_3 and 10 wt% SnO_2 planar target was developed in a previous study by optimizing the substrate temperature, process pressure and sputter power [21–23]. The best results were achieved by applying a power density of 0.4 W/cm^2 , 50°C chamber temperature and 0.26 Pa process pressure with no oxygen gas flow into the system during sputtering process. For all processes Argon was used as the sputter gas at 30 sccm flow rate. In this study the previously optimized ITO process with no oxygen gas flow into the system during sputtering and a resulting layer thickness of 77 nm is taken as reference point (ITO_{Ref}). To further improve electron mobility while reducing sheet resistance and absorptance of the ITO thin films, the oxygen flow rate during the sputter process is increased to 0.2 sccm and 0.4 sccm with all other parameters kept constant. The sheet resistance was measured using the Van der Pauw method on glass substrates [24].

The sheet resistance of the as deposited ITO_{Ref} (0 sccm oxygen) and ITO_{O_2} (0.2 sccm oxygen) films on glass are similar with a slight decrease for the ITO_{O_2} film. Further increasing the oxygen flow rate up to 0.4 sccm results in a sharp increase of the sheet resistance from $\sim 60 \Omega/\text{sq}$ up to $128 \Omega/\text{sq}$ (Fig. 1a). The charge carrier density and mobility of the films were extracted via Hall effect measurements. Increasing the oxygen flow rate resulted in an increase of electron mobility from $27.3 \text{ cm}^2/\text{Vs}$ up to $53.4 \text{ cm}^2/\text{Vs}$ and decrease of the charge carrier concentration from $4.43 \times 10^{20} \text{ cm}^{-3}$ to $1.37 \times 10^{20} \text{ cm}^{-3}$ (Fig. 1b).

Increasing the oxygen pressure extinguishes oxygen vacancies, which usually act as electron donors to the conduction band but act as ionized impurities limiting the scattering time and thus the mobility of the electrons. The sheet resistance is calculated from the inverse product

of mobility, charge carrier concentration and the layer thickness (see Equation (1)).

$$R_{\text{sh}} = \frac{1}{e\mu_e N_e d} \quad 1$$

In Equation (1), R_{sh} is the sheet resistance, e the elementary electron charge and μ_e the electron mobility, N_e the free carrier concentration and d the sample thickness.

The absorptance ($1-R-T$) of the ITO films in $450\text{--}1600 \text{ nm}$ wavelength range is reduced by increasing the oxygen flow rate during sputtering process (Fig. 1c). The optical bandgap values are calculated from respective Tauc plot fits. The optical bandgap shows a red shift with increasing oxygen flow rate (Fig. 1d).

Due to the low sheet resistance compared to 0.4 sccm and decreased absorptance, ITO films sputtered with 0.2 sccm oxygen flow rate (ITO_{O_2}) as well as the ITO films sputtered with 0 sccm oxygen flow rate (ITO_{Ref}) were selected for implementation as top TCO into perovskite silicon tandem solar cell with a structure as described in Schulze et al. [25] (Fig. 2).

The solar cells are characterized with current voltage (I - V) measurements in forward and reverse scan directions under a sun simulator. ITO_{O_2} thin films result in average $\sim 1 \text{ mA/cm}^2$ higher short circuit current density (j_{SC}) compared to solar cells with ITO_{Ref} both in forward and reverse scan direction I - V measurements. The increase in j_{SC} can be explained by reduced absorptance (Figs. 3–1c).

Despite the improvement in j_{SC} , the average fill factor (FF) decreases from 70% to 76% for ITO_{Ref} group to 57% and 65% for ITO_{O_2} group, for forward and reverse scan directions, respectively (Fig. 3). This might be due to less efficient carrier transport for the more oxygen rich TCO caused either by less efficient lateral transport (higher R_{sheet}) and/or less efficient vertical transport (contact resistivity to electron contact or top metal electrode). The reduced FF could also be an effect of changed current matching point for oxygen rich ITO [26]. Since reduced FF values for the ITO_{O_2} group balances out the effect of improvement in j_{SC} , no improvement in power conversion efficiency could be observed.

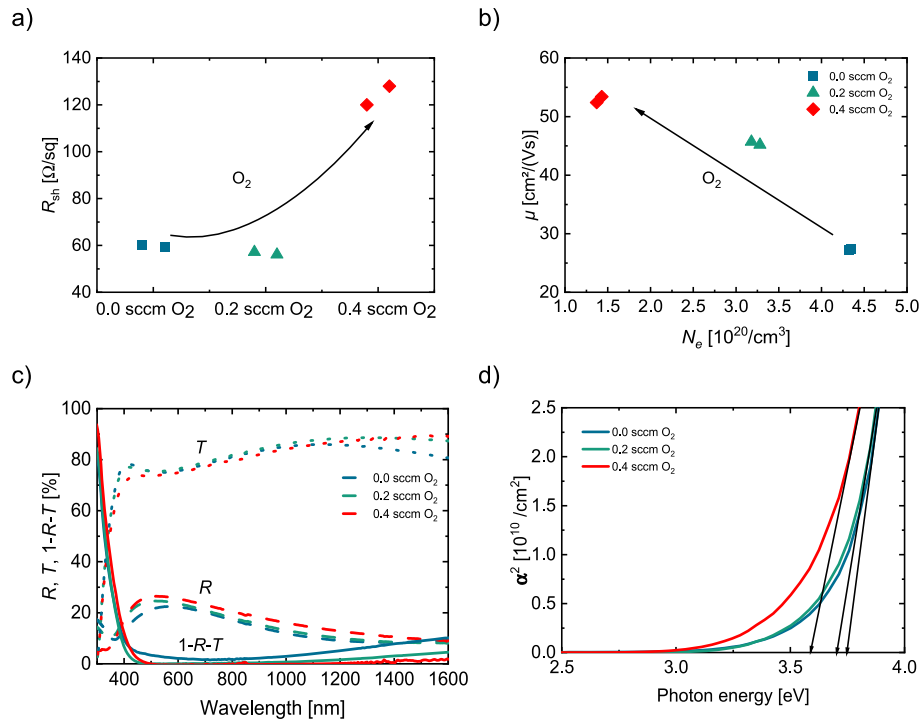


Fig. 1. ITO films on glass with varying oxygen flow rate (0 sccm , 0.2 sccm , 0.4 sccm) during sputter process. Lowest sheet resistance is obtained with 0.2 sccm flow rate (a) Mobility of the films decrease by increasing charge carrier density as expected (b) absorptance of the films can be reduced by increasing oxygen flow rate (c) optical bandgap reduces with the increasing oxygen flow rate (d).

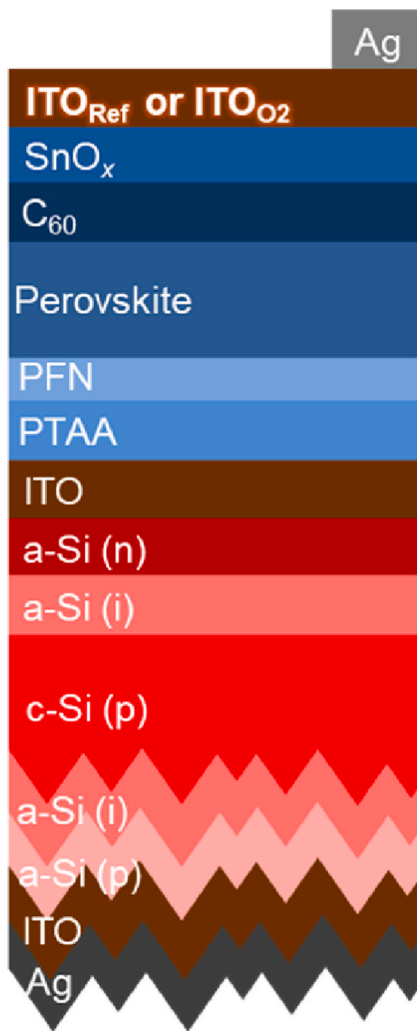


Fig. 2. Tandem solar cell stack sketch. The silicon bottom solar cell has planar front and random pyramid texturing at the rear side. The ITO layer is changed between two groups (ITO_{Ref} or ITO_{O2}) while keeping the rest of the stack the same.

The contact resistivity between ITO and the PVD Ag metallization is typically < 1 mOhmcm² and thus not a relevant series resistance contribution in our devices and ITO_{O2} thin films exhibit a very similar

sheet resistance compared to the ITO_{Ref} (Fig. 1a) [27]. Thus, one of the reasons for the higher losses for the ITO_{O2} group solar cells might be a poor contact formation between ITO_{O2} and the SnO_x buffer layer. On the other hand, the problem is not present for the ITO_{Ref}. Therefore, to address this problem an oxygen poor ITO interlayer is introduced between ITO and SnO_x. As shown in Fig. 1, such an oxygen poor ITO layer has a higher charge carrier concentration, which can help to reduce the effective Schottky barrier with lower charge carrier concentration of the oxygen rich ITO layer. A similar approach using the same deposition tool and ITO target has proven useful recently to balance optical and electrical losses of TCO electrodes in silicon heterojunction solar cells [28].

Roughness estimations from spectroscopic ellipsometry measurements are done for single ITO_{O2} layers with various thicknesses (Table 1). The roughness measurements indicate that the roughness is relatively high compared to the nominal film thickness for film thicknesses below 20 nm and that layer thicknesses above 8 nm are necessary to have a closed compact film.

By taking the electro-optical properties, contact resistivity and roughness results into account an oxygen poor and an oxygen rich layer in the stacks are subsequently sputtered in one uninterrupted process. For the total final thicknesses of all the stack film variations, 75 nm are aimed (Fig. 4). Various thicknesses of thin layers of oxygen poor (ITO_{Ref}) (15 nm, 25 nm) and oxygen rich (ITO_{O2}) top films (60 nm, 50 nm) are combined to form the stack.

The sheet resistances of all layer stacks range between the sheet resistance values of ITO_{Ref} and ITO_{O2} thin films, as expected (Fig. 5). The sheet resistance values for ITO_{Ref} and ITO_{O2} are slightly different compared to the first set of experiments (±5 Ω/sq) (Figs. 1a and 5a). This can be attributed to the slight variations that could occur between two experimental sets. The stack with 15 nm interlayer exhibits higher mobilities compared to stack with 25 nm, but slightly lower compared to ITO_{O2} film (Fig. 5b). The absorptance can be significantly reduced for

Table 1

Nominal thickness and roughness values of ITO_{O2} films estimated from spectroscopic ellipsometry measurements (SE).

Nominal thickness [nm]	SE thickness [nm]	SE roughness [nm]
2	2.2	2.8
4	3.5	4
6	4.9	5.4
8	6.4	7
10	8.9	6.5
12	11.1	6.4
16	15.2	6.6
20	19.4	7
25	25.2	3

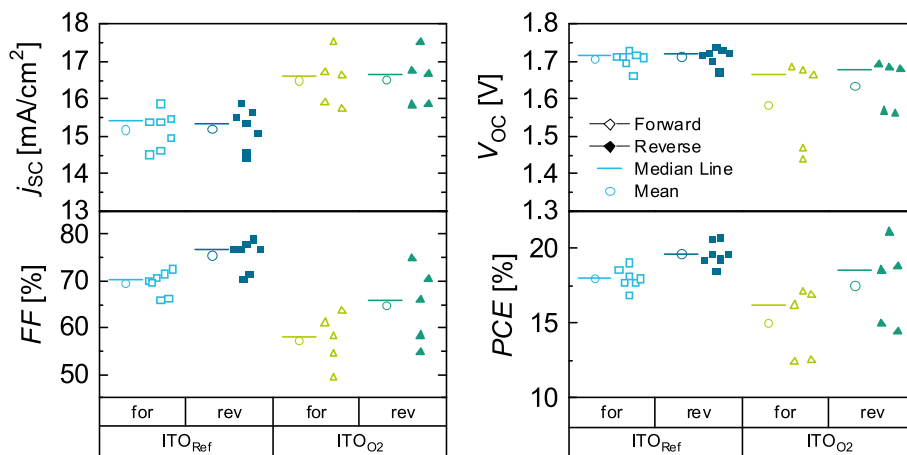


Fig. 3. Photovoltaic parameters of the perovskite silicon tandem solar cells with two different ITO films. The I–V measurements are conducted with non-adjusted spectrum. j_{sc} improves when ITO_{O2} films are implemented.

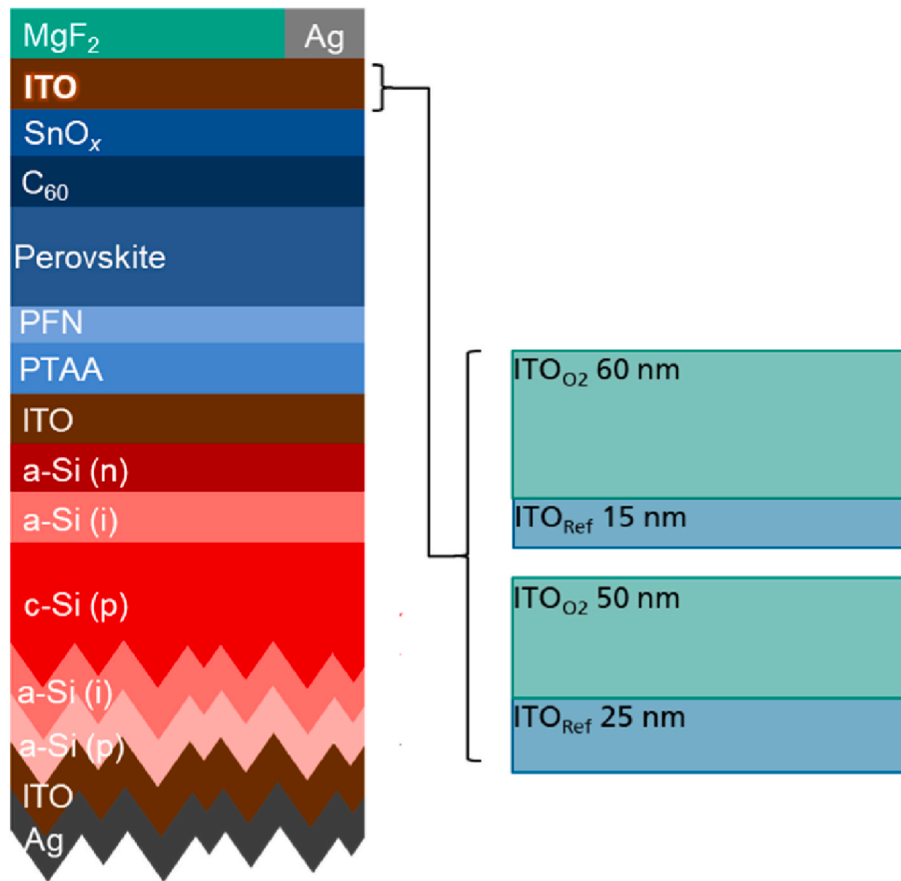


Fig. 4. Sketches of perovskite silicon tandem solar cell configuration and stack variations of the top ITO thin film.

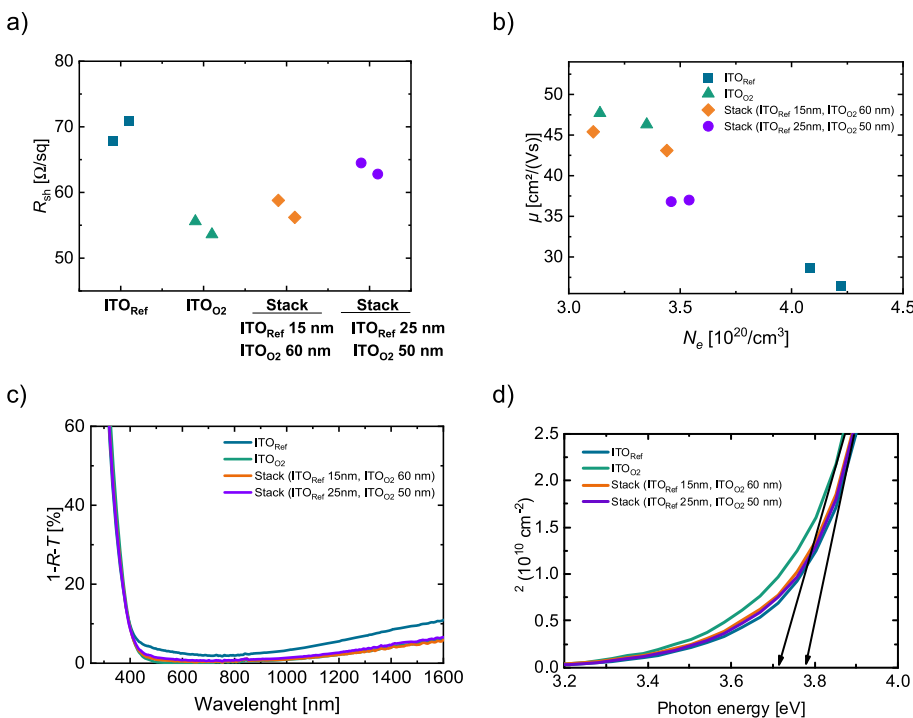


Fig. 5. 75 nm thick ITO films and stacks with varying oxygen poor (0 sccm, ITO_{Ref}) and oxygen rich (0.2 sccm, ITO_{O_2}) layer thickness in stack (15 nm, 25 nm). Comparing the stack samples, the stack with 15 nm thin oxygen poor layer features the lower sheet resistance (a) and the higher mobility close to ITO_{O_2} thin film (b) and a lower absorbance (c). The optical bandgap reduces with the increasing oxygen flow rate. Similar optical bandgaps are obtained for stack processes and ITO_{Ref} (d).

the 450–1600 nm wavelength range also for the stack groups, as observed with ITO_{O_2} , with only a slight increase by increasing oxygen deficit layer share in the stack (Fig. 5c). The optical bandgaps of the

stack layers are similar to the optical bandgap of ITO_{Ref} (Fig. 5d).

Since the stack comprising a 15 nm oxygen deficient layer share (ITO_{Stack}) shows first-rate electro-optical properties and a closed layer

can be assumed at this thickness, it is chosen for implementation into perovskite silicon tandem solar cells.

In a next step the ITO stack approach was investigated on the tandem device level. This time a perovskite absorber with a slightly lower bandgap was implemented as recommended by simulation (change from 1.68 eV to 1.64 eV) and a MgF₂ anti-reflective coating layer is added to the stack [9]. Tandem solar cells with oxygen poor single-layer (ITO_{Ref}), oxygen rich single-layer (ITO_{O2}) and stack with 15 nm oxygen poor interlayer (ITO_{Stack}) are compared. The lower bandgap perovskite absorber and the anti-reflective coating resulted in a ~3 mA/cm² increase of *j*_{SC} for both ITO_{Ref} and ITO_{O2} processes compared to the first set of experiments (Fig. 6a). Almost no hysteresis is observed, and similar results are obtained for forward and reverse direction *I*-*V* measurements. The highest absolute efficiency is obtained for ITO_{Stack} process as

25.6% in both scan directions.

As in the first set of experiments, increasing the O₂ content in the ITO improves the *j*_{SC} considerably. ITO_{Ref} group has an average *j*_{SC} of 19.3 ± 0.4 mA/cm² whereas for ITO_{O2} group it is 19.9 ± 0.3 mA/cm². Reduced absorptance could be one of the possible reasons for the increased average *j*_{SC} (Fig. 5c). The ITO_{Stack} group has an average *j*_{SC} of 19.8 ± 0.2 mA/cm², which is comparable to the current of the ITO_{O2} group. To the best of our knowledge, in literature, up to now the high efficiency perovskite silicon tandems with such a silicon hetero-junction structure with planar front and random pyramid textured rear side reported *j*_{SC} values up to 19.29 mA/cm² and front side nanotextured 19.48 mA/cm², whereas both side textured ones up to 19.8 mA/cm² [29–31]. According to spectrometric characterization for all three groups the silicon bottom solar cell is limiting the overall tandem device current (Fig. S1) [26,32].

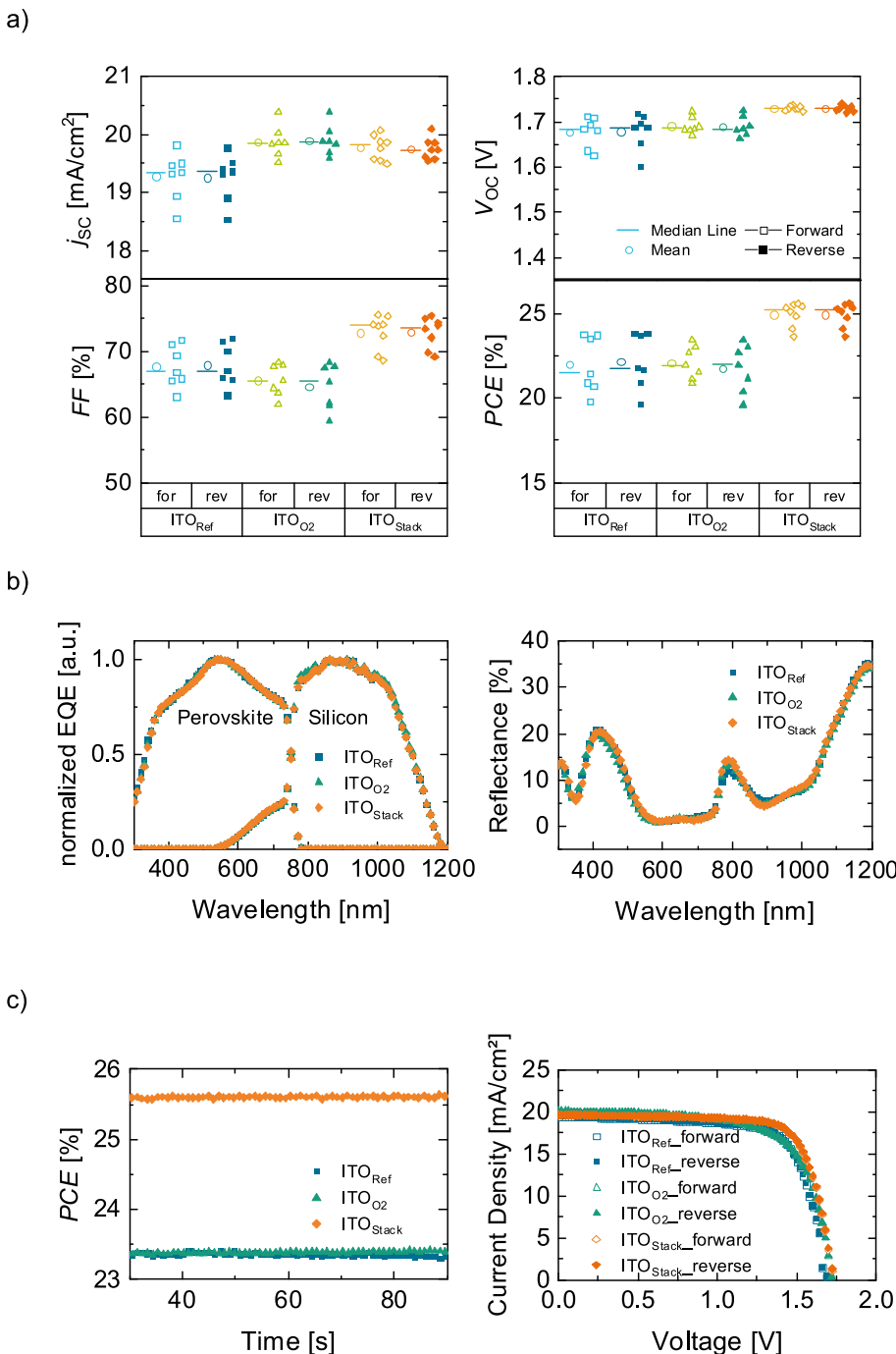


Fig. 6. Photovoltaic parameters of the perovskite silicon tandem solar cells with three different ITO films show that highest efficiency could be achieved with ITO_{Stack} group mainly due to *j*_{SC} and FF increase (a) EQE and reflectance of all three tandem solar cells for all ITO films are similar (b) The PCE tracked over 90 s at maximum power point voltage shows that the highest efficiency is obtained with ITO_{Stack} (left) and IV-curves of highest efficiency solar cell per group shows that ITO_{Ref} and ITO_{O2} groups have rounder I-V curve shape (right) (c).

However, samples from ITO_{Stack} and ITO_{O₂} groups are closer to the current matching point compared to the sample from ITO_{Ref} group (Fig. S1), which could also be an explanation for the higher average j_{SC} .

EQE and reflection measurements were conducted on the highest efficiency solar cell per group (Fig. 6b). As measuring the absolute EQE is already challenging for single junction solar cells [33], especially if meta-stable materials such as perovskites are involved [34,35], and generally for tandem solar cells [36], normalized EQEs are shown. Except a slight increase in 780–790 nm range for ITO_{O₂} the shapes of the EQE curves for all ITO variations are similar to each other within the measurement uncertainties.

Average FF of 68%, 65% and 73% are obtained for ITO_{Ref}, ITO_{O₂} and ITO_{Stack} respectively. FF are lower compared to first set of experiments for ITO_{Ref} and ITO_{O₂} groups. This decrease can be related with changing the perovskite composition and bandgap. The lower bandgap perovskite absorber (1.64 eV) that is used in the second set of experiments results in improved current matching compared to the absorber with 1.68 eV used in the first set of experiments [9,32].

3. Discussion

Using the stack design, the efficiency of the tandem solar cells could be considerably increased. The main motivation for the stack design had been to achieve the current enhancement observed for the oxygen rich ITO, without the detrimental effects on FF . With the stack design an increase of the average j_{SC} compared to the reference ITO process from $19.3 \pm 0.4 \text{ mA/cm}^2$ up to $19.8 \pm 0.2 \text{ mA/cm}^2$ was achieved. Despite the simple silicon hetero junction design, excellent high j_{SC} can be reached that is among the highest for planar perovskite silicon tandem solar cells and even slightly higher than the currently highest efficient tandem published with an advanced nano-optical bottom solar cell design [30].

The stack design even exceeded the reference ITO for both the FF and the V_{OC} . The stack design improved the average FF from 68% to 73% and the average V_{OC} from 1.68 V to 1.73 V compared to the reference ITO. We hypothesised that too low doping in the oxygen rich ITO caused the lower FF . Therefore we also determined the contact resistivity between ITO and SnO_x for ITO_{Ref} and ITO_{O₂} via μ -TLM of sandwich-like samples having the structure Ag/ITO/SnO_x/ITO/glass [37]. μ -TLM on structured multi-layer stacks is very challenging and several prepared patterns did not produce any result. Where a contact resistance could be measured, the contact resistance was clearly lower for the ITO_{O₂}. However, the overall level was in the range of 10–80 m Ωcm^2 . If the measurement results are correct, this would mean that the impact of this specific contact resistance onto the total series resistance of the entire cell is only minor. To further investigate, we also determined the total series resistances of the highest efficiency solar cell per group from the slope of the I - V curves at the V_{OC} point. To validate the findings, series resistances were additionally determined from a comparison of I - V curves and Suns- V_{OC} measurements similar to the method principle described in Refs. [38,39]. The slope at the V_{OC} results in total series resistances for the highest efficiency tandem solar cells of 7–9 Ωcm^2 . Series resistances extracted with the Suns- V_{OC} method are in the range of 2–6 Ωcm^2 . No trend in the series resistance can be observed for the ITO variations within the measurement uncertainty. One has to keep in mind, however, that these techniques are also not well established for meta-stable tandem devices. Putting everything into perspective, most likely the decrease in contact resistance due to higher doping is not the only effect causing the trends in FF in Fig. 6a. The slightly higher V_{OC} and FF of ITO_{Stack} group is pointing towards a possible reduced recombination effect and reduced transport losses. Moreover, the rounder I - V curve shape for ITO_{Ref} and ITO_{O₂} in Fig. 6c could be due to a lateral inhomogeneity within the measured solar cell area. More characterization and simulation work – also for the tandem solar cells' behaviour in the various characterization scenarios – is necessary to elucidate these questions in future work.

4. Conclusion

In this study two optimized ITO film stacks are developed that provide improved electro-optical properties. Initially, an optimized doping level for the ITO is found to provide low absorptance and moderate sheet resistance. Doping of the ITO is controlled via the oxygen flow rate during the sputtering process. It was found that 0.2 sccm (ITO_{O₂}) reduces the absorptance of the films and slightly reduces the sheet resistance compared to oxygen deficit layer with 0 sccm (ITO_{Ref}). Higher flow rate resulted in a sharp increase of the sheet resistance. In the first set of experiments, the improved optical properties of the ITO_{O₂} thin films resulted in a significant j_{SC} increase of the tandem solar cells yet slightly lower FF values were obtained for this group. This pointed towards a possible resistive loss caused by ITO_{O₂}, which might be poor contact formation with SnO_x in combination with other tandem effects such as current matching condition change. For improving the electrical contact of the ITO with SnO_x layer, in the second step of the optimization, a stack approach is developed. In the stack approach a highly doped (oxygen deficit) layer is combined with a moderately doped layer. A second experiment is conducted to compare the highly doped, moderately doped, and stacked ITO layers. Higher j_{SC} could be obtained with both ITO_{O₂} and ITO_{Stack} groups compared to ITO_{Ref}. The improvement of j_{SC} originated from optical improvement and tandem current-matching point effects. ITO_{Stack} group also exhibited higher FF compared to other groups. All in all, efficiency of 25.6% can be achieved with the ITO_{Stack} thin films with highest absolute FF . The improvement in electro-optical properties of the optimized ITO layers result in a good combination of moderate sheet resistance and low absorptance.

Our findings can stimulate further in-depth analysis of losses and kinetics in multi-layer perovskite silicon tandem solar cells. In the specific case at the SnO_x/ITO interface, findings can help to define a tailored sputter deposition process and improve device performance. Moreover, the multi-stack approach is not limited to tandem devices with planar front and can be transferred to fully textured perovskite silicon tandem devices.

5. Material and methods

5.1. Silicon bottom solar cell

250 μm -thick p-type float zone silicon wafers with a base resistivity of 1 Ωcm (Siltronic) are used for the silicon bottom solar cells. The back side of the wafer is etched with a pyramidal texture by using potassium hydroxide (KOH). After RCA cleaning and subsequent HF dipping in 1% aqueous solution to remove the SiO₂, an intrinsic doped amorphous silicon passivation layer stack is deposited on both sides (plasma-enhanced chemical vapor deposition (PECVD), Indeotec cluster tool). The thickness of the undoped layer is 6.0 nm while the thickness of the n-doped and p-doped amorphous silicon layer are 12 nm.

The amorphous silicon is deposited in a parallel-plate PECVD reactor (13.56 MHz, 200 °C) using mixtures of silane (SiH₄), hydrogen (H₂), phosphine (PH₃), and trimethyl boron (TMB). ITO (In₂O₃/SnO₂ ¼ 90/10 wt%) is DC sputtered on both sides using argon and oxygen mixtures (Oxford Instruments cluster tool). 195 nm ITO is deposited on the textured back side. Approximately 80 nm of ITO is sputtered on the planar front side. The front side ITO is sputtered by using a shadow mask with 4 windows of 6 mmx6 mm size. Each window defines the individual solar cell areas on a substrate. Ag (1000 nm) is deposited on the textured side as the rear contact. The wafers are cut into substrates of size 2.5 cmx2.5 cm (each containing 4 individual solar cell area defined by the ITO deposited through the shadow mask).

5.2. Perovskite top solar cell

The perovskite top solar cell has p-i-n polarity with a layer stack of interconnection ITO/PTAA/PFN/perovskite/C₆₀/SnO_x/ITO, where the

top ITO is varied. The silicon bottom solar cell substrates are UV-ozone treated for 15 min and blown with N₂. All following steps until except ITO sputtering are done under inert glovebox atmosphere. PTAA (3 mg/mL in Toluene) is spin-coated (6000 rpm for 30 s) and annealed at 100 °C for 10 min. PFN (0.5 mg/mL in Methanol) layer is spin coated (5000 rpm for 20 s) on top of PTAA. The higher bandgap perovskite (1.68 eV) solution is prepared by mixing FAI, CsI, PbBr₂, PbI₂ in a DMF:DMSO (4:1 vol ratio) in stoichiometric amounts and stirred at 60 °C overnight to obtain FA_{0.75}Cs_{0.25}Pb(I_{0.8}Br_{0.2})₃ as described in Schulze, Bett et al. [25]. The perovskite solution is spin coated at one step (1000 rpm for 10s, 5000 rpm for 20s, 150 µL precursor solution, 200 µL chlorobenzene after 25 s - over last 5 s). The lower bandgap perovskite is prepared according to triple cation perovskite preparation methods described in literature [40,41]. For the lower bandgap (1.64 eV) perovskite first, 1.2 M MAPbBr₃ solution (with 10% Pb excess), 1.2 M FAPbI₃ solution (with 10% Pb excess) in mixture of DMF:DMSO (4:1 vol ratio) and 1.5 M CsI solution in DMSO are prepared and stirred overnight at room temperature. The FAPbI₃ and MAPbBr₃ solutions are then mixed in a 83:17 ratio. Finally, 5 vol-% of CsI is added to the perovskite precursor to obtain Cs_{0.05}(FA_{0.83}MA_{0.17})_{0.95}Pb(I_{0.83}Br_{0.17})₃ perovskite composition. The perovskite solution is spin coated in one step (4000 rpm 35 s, ramp 3 s 150 µL perovskite solution, 300 µL ethyl acetate anti-solvent after 10 s). Perovskite layers are annealed for 1 h at 100 °C after spin coating. The perovskite layer thicknesses are around 400 nm and 450 nm for high and low bandgap perovskites respectively. A 15 nm C₆₀ is thermally evaporated (0.2 Å/s) on top of the perovskite layer. 20 nm SnO_x is deposited via ALD at 80 °C. Top ITO layers are deposited via DC magnetron sputtering with set parameters of power density at 0.4 W/cm², process pressure of 0.26 Pa and the substrate temperature at 50 °C. Argon is used as sputtering gas (30 sccm flow rate). A circular In₂O₃:SnO₂ target of 25.4 cm diameter size with the composition ratio of is 90:10 wt% is used. The target purity is 99.99%. The flow rate of the oxygen gas was varied to tune film properties. As the last steps 200 nm Ag and 100 nm MgF₂ layers are deposited via evaporation. The Ag was evaporated through shadow masks defining the solar cell areas on the substrate (0.25 cm² solar cell area, 4 solar cells on each substrate). The MgF₂ was evaporated on full area of the substrates.

5.3. Characterization

5.3.1. Spectroscopic ellipsometry

The thicknesses and optical constants of the ITO thin films are determined via spectroscopic ellipsometry by fitting a Drude-Tauc-Lorentz model by taking the roughness into account. ITO thin films that are used in spectroscopic ellipsometry measurements are deposited on silicon substrates.

5.3.2. UV-Vis-NIR spectroscopy

Reflectance and transmittance data are extracted using a Lambda 950 spectrophotometer from PerkinElmer with an integrating sphere (scanning the wavelength range of 250–1200 nm using a step size of 2 nm). The absorbance is calculated from reflectance-transmittance data (1-R-T). The optical bandgaps of the ITO thin films are calculated from the absorbance data. ITO thin films deposited on glass are used for UV-Vis spectroscopy.

5.3.3. Electrical properties

The sheet resistances of the ITO thin films are estimated by using Van der Pauw method on glass samples covered with ITO and mobility and carrier density extracted via Hall effect measurement.

5.3.4. μ -STLM measurements

The measurement stacks are made of glass, 260 nm thick ITO, 10 + 10 nm thick SnO_x (lower 10 nm SnO_x annealed in vacuum at 300 °C), ~75 nm ITO_{Ref} or ITO_{O2} and 100 nm Ag. A plasma-FIB (focused ion beam) technique was used to prepare the μ -TLM test patterns by ablation

of the Ag/ITO_{Ref}/SnO_x layers, leaving behind contacts with approximate area of 400 × 50 µm² and contact pad spacings between 50 µm and 250 µm. The contact resistivities at the ITO/SnO_x interface are calculated from the total resistance and contact area of the measurement.

5.3.5. Current voltage (*I*-*V*) and EQE measurements

The first set of current-voltage (*I*-*V*) measurements of perovskite silicon tandem solar cells are conducted using a LED sun simulator (Wavelabs, Sinus-220) where the light intensity is calibrated to 1 sun by a silicon reference solar cell using a spectrally non-adjusted fitted AM1.5 g spectrum. For the second set of measurements, prior to *I*-*V* measurements spectral response is measured for one solar cell of each group. Chopped light (frequency ~ 130 Hz) of a Xenon lamp is directed to a double monochromator. Monochromatic light is directed to the tandem device. The measurement light spot is smaller than the active tandem solar cell area. For the measurement of the perovskite top cell and the silicon bottom cell infrared and blue LEDs, respectively, are used to bring the sub-cell to be measured into current limitation. The signal is directed to a transimpedance amplifier and a lock-in amplifier. The transimpedance amplifier allows to apply a bias voltage to the tandem solar cell. Bias voltages of ~680 mV and ~1080 mV are used to measure the top and bottom solar cell, respectively, in order to have the cell to be measured approximately in short-circuit conditions. Details on spectral response measurements of tandem solar cells can be found in Ref. [36]. Note, that for tandem solar cells the measurement of absolute spectral response is challenging [36]. If perovskite is involved dynamic effects lead to dependence of the absolute spectral response on measurement conditions [34,35]. However, for adjusting the sun simulator only relative spectral responses are required. A Wacom sun simulator equipped with a filtered Xenon lamp (UV and visible light) and a filtered Halogen lamp (infrared light) is used which can be adjusted individually. The relative spectral responses and the spectra of the lamps were used to determine the lamp intensities by solving the linear equation system described in Ref. [26]. Lamp intensities are set by adjusting the current of two filtered WPVS reference solar cells. A Keithley 2400 source meter is used to record the *I*-*V* curves in forward and reverse scan direction. Voltage range was -0.1 V–1.9 V, step size was 20 mV with a scan speed of ~33 mV/s. The active area of 0.25 cm² is defined by a shadow mask. Each solar cell is measured several times until a stabilized efficiency is reached. The parameters of the best mean efficiency of forward and reverse scan *I*-*V* measurement are presented in the plots. To determine stabilized efficiency the maximum power point voltage is applied, and the current is recorded over time. The series resistance is calculated from the slope at the *V*_{OC} by taking 6 data points at the *I*-*V* curve (3 before and 3 after the *V*_{OC}).

Details on spectrometric characterization can be found in Ref. [32].

CRedit authorship contribution statement

Özde Ş. Kabaklı: Writing – review & editing, Writing – original draft, Investigation, Data curation. **Jakob Kox:** Investigation, Data curation. **Leonard Tutsch:** Writing – review & editing, Supervision, Investigation, Data curation. **Minasadat Heydarian:** Writing – review & editing, Data curation. **Alexander J. Bett:** Writing – review & editing, Data curation. **Stefan Lange:** Data curation. **Oliver Fischer:** Data curation. **Christian Hagendorf:** Supervision. **Martin Bivour:** Writing – review & editing, Supervision. **Martin Hermle:** Writing – review & editing, Supervision. **Patricia S.C. Schulze:** Writing – review & editing, Supervision. **Jan Christoph Goldschmidt:** Writing – review & editing, Supervision.

Declaration of competing interest

The authors declare that they have no known competing financial interests or personal relationships that could have appeared to influence the work reported in this paper.

Data availability

Data will be made available on request.

Acknowledgements

Ö.Ş. Kabaklı, P.S.C. Schulze, M. Heydarian optimized the perovskite top solar cell fabrication. Ö.S. Kabaklı fabricated the perovskite silicon tandem solar cells. J. Kox, L. Tutsch optimized the TCO thin films and performed the characterization of the thin films. O. Fischer investigated the series resistance of the cells. S. Lange investigated the contact resistivity of the ITO-SnO_x interface. A.J. Bett supervised the current-voltage characterization of the tandem solar cells. All authors participated in proofreading as well as correcting. J.C. Goldschmidt, P.S.C. Schulze, C. Hagendorf, M. Bivour, M. Hermle supervised the project. The authors would like to thank K. Fischer, M.A.A. Mahmoud, J. Aulich and K. Abrorov for support during the measurements and technical issues.

This work was supported by Fraunhofer Gesellschaft, Germany via the Fraunhofer MANITU Lighthouse Project. Ö.Ş.K. gratefully acknowledges scholarship from the Dr. Ruth Heerdt Stiftung.

Appendix A. Supplementary data

Supplementary data to this article can be found online at <https://doi.org/10.1016/j.solmat.2023.112246>.

References

- [1] T. Niewelt, B. Steinhauser, A. Richter, B. Veith-Wolf, A. Fell, B. Hammann, N. E. Grant, L. Black, J. Tan, A. Youssef, J.D. Murphy, J. Schmidt, M.C. Schubert, S. W. Glunz, Reassessment of the intrinsic bulk recombination in crystalline silicon, *Sol. Energy Mater. Technol.* 235 (2022), 111467, <https://doi.org/10.1016/j.solmat.2021.111467>.
- [2] Best Research-Cell, Efficiency Chart, 2022.
- [3] N.N. Lal, Y. Dkhissi, W. Li, Q. Hou, Y.-B. Cheng, U. Bach, Perovskite tandem solar cells, *Adv. Energy Mater.* 7 (2017), 1602761, <https://doi.org/10.1002/aenm.201602761>.
- [4] B. Chen, X. Zheng, Y. Bai, N.P. Padture, J. Huang, Progress in tandem solar cells based on hybrid organic-inorganic perovskites, *Adv. Energy Mater.* 7 (2017), 1602400, <https://doi.org/10.1002/aenm.201602400>.
- [5] S. de Wolf, J. Holovsky, S.-J. Moon, P. Löper, B. Niesen, M. Ledinsky, F.-J. Haug, J.-H. Yum, C. Ballif, Organometallic halide perovskites: sharp optical absorption edge and its relation to photovoltaic performance, *J. Phys. Chem. Lett.* 5 (2014) 1035–1039, <https://doi.org/10.1021/jz500279b>.
- [6] E.L. Unger, L. Kegelmann, K. Suchan, D. Sörell, L. Korte, S. Albrecht, Roadmap and roadblocks for the band gap tunability of metal halide perovskites, *J. Mater. Chem.* 5 (2017) 11401–11409, <https://doi.org/10.1039/C7TA00404D>.
- [7] Q. Chen, N. de Marco, Y. Yang, T.-B. Song, C.-C. Chen, H. Zhao, Z. Hong, H. Zhou, Under the spotlight: the organic-inorganic hybrid halide perovskite for optoelectronic applications, *Nano Today* 10 (2015) 355–396, <https://doi.org/10.1016/j.nantod.2015.04.009>.
- [8] K. Jäger, L. Korte, B. Rech, S. Albrecht, Numerical optical optimization of monolithic planar perovskite-silicon tandem solar cells with regular and inverted device architectures, *Opt Express* 25 (2017) A473–A482, <https://doi.org/10.1364/OE.25.00A473>.
- [9] C. Messmer, B.S. Goraya, S. Nold, P.S. Schulze, V. Sittinger, J. Schön, J. C. Goldschmidt, M. Bivour, S.W. Glunz, M. Hermle, The race for the best silicon bottom cell: efficiency and cost evaluation of perovskite-silicon tandem solar cells, *Prog. Photovoltaics Res. Appl.* (2020), <https://doi.org/10.1002/pip.3372>.
- [10] Q. Xu, Y. Zhao, X. Zhang, Light management in monolithic perovskite/silicon tandem solar cells, *Sol. RRL* 173 (2019), 1900206, <https://doi.org/10.1002/solr.201900206>.
- [11] M. Morales-Masis, S. de Wolf, R. Woods-Robinson, J.W. Ager, C. Ballif, Transparent electrodes for efficient optoelectronics, *Adv. Electron. Mater.* 3 (2017), 1600529, <https://doi.org/10.1002/aenm.201600529>.
- [12] H. Hosono, H. Ohta, M. Orita, K. Ueda, M. Hirano, Frontier of transparent conductive oxide thin films, *Vacuum* 66 (2002) 419–425, [https://doi.org/10.1016/S0042-207X\(02\)00165-3](https://doi.org/10.1016/S0042-207X(02)00165-3).
- [13] H. Kanda, A. Uzum, A.K. Baranwal, T.A.N. Peiris, T. Umeyama, H. Imahori, H. Segawa, T. Miyasaka, S. Ito, Analysis of sputtering damage on I–V curves for perovskite solar cells and simulation with reversed diode model, *J. Phys. Chem. C* 120 (2016) 28441–28447, <https://doi.org/10.1021/acs.jpcc.6b09219>.
- [14] H. Lei, M. Wang, Y. Hoshi, T. Uchida, S. Kobayashi, Y. Sawada, Comparative studies on damages to organic layer during the deposition of ITO films by various sputtering methods, *Appl. Surf. Sci.* 285 (2013) 389–394, <https://doi.org/10.1016/j.apsusc.2013.08.065>.
- [15] E. Aydin, C. Altinkaya, Y. Smirnov, M.A. Yaqin, K.P. Zanoni, A. Paliwal, Y. Firdaus, T.G. Allen, T.D. Anthopoulos, H.J. Bolink, M. Morales-Masis, S. de Wolf, Sputtered transparent electrodes for optoelectronic devices: induced damage and mitigation strategies, *Matter* 4 (2021) 3549–3584, <https://doi.org/10.1016/j.matt.2021.09.021>.
- [16] K.O. Brinkmann, J. Zhao, N. Pourdavoud, T. Becker, T. Hu, S. Olthof, K. Meerholz, L. Hoffmann, T. Gahlmann, R. Heiderhoff, M.F. Oszajca, N.A. Luechinger, D. Rogalla, Y. Chen, B. Cheng, T. Riedl, Suppressed decomposition of organometal halide perovskites by impermeable electron-extraction layers in inverted solar cells, *Nat. Commun.* 8 (2017), 13938, <https://doi.org/10.1038/ncomms13938>.
- [17] H.H. Park, Inorganic materials by atomic layer deposition for perovskite solar cells, *Nanomaterials* 11 (2021), <https://doi.org/10.3390/nano11010088>.
- [18] F. Sahli, J. Werner, B.A. Kamino, M. Bräuninger, R. Monnard, B. Paviet-Salomon, L. Barraud, L. Ding, J.J. Diaz Leon, D. Sacchetto, G. Cattaneo, M. Despeisse, M. Boccard, S. Nicolay, Q. Jeangros, B. Niesen, C. Ballif, Fully textured monolithic perovskite/silicon tandem solar cells with 25.2% power conversion efficiency, *Nat. Mater.* 17 (2018) 820–826, <https://doi.org/10.1038/s41563-018-0115-4>.
- [19] K.A. Bush, S. Manzoor, K. Frohna, Z.J. Yu, J.A. Raiford, A.F. Palmstrom, H.-P. Wang, R. Prasanna, S.F. Bent, Z.C. Holman, M.D. McGehee, Minimizing current and voltage losses to reach 25% efficient monolithic two-terminal perovskite-silicon tandem solar cells, *ACS Energy Lett.* 3 (2018) 2173–2180, <https://doi.org/10.1021/acseenergylett.8b01201>.
- [20] K.A. Bush, A.F. Palmstrom, Z.J. Yu, M. Boccard, R. Cheacharoen, J.P. Mailoa, D. P. McMeekin, R.L.Z. Hoye, C.D. Bailie, T. Leijtens, I.M. Peters, M.C. Minichetti, N. Rolston, R. Prasanna, S. Sofia, D. Harwood, W. Ma, F. Moghadam, H.J. Snaith, T. Buonassisi, Z.C. Holman, S.F. Bent, M.D. McGehee, 23.6%-efficient monolithic perovskite/silicon tandem solar cells with improved stability, *Nat. Energy* 2 (2017), 17009, <https://doi.org/10.1038/nenergy.2017.9>.
- [21] A.J. Bett, Perovskite Silicon Tandem Solar Cells: Two-Terminal Perovskite Silicon Tandem Solar Cells Using Optimized N-I-P Perovskite Solar Cells, Dissertation, Fraunhofer Verlag, Stuttgart, 2020.
- [22] P.S.C. Schulze, High Band Gap Perovskite Absorbers for Application in Monolithic Perovskite Silicon Tandem Solar Cells, Inauguraldissertation, 2020.
- [23] A.J. Bett, K.M. Winkler, M. Bivour, L. Cojocar, Ö.Ş. Kabaklı, P.S.C. Schulze, G. Siefert, L. Tutsch, M. Hermle, S.W. Glunz, J.C. Goldschmidt, Semi-transparent perovskite solar cells with ITO directly sputtered on spiro-OMeTAD for tandem applications, *ACS Appl. Mater. Interfaces* 11 (2019) 45796–45804, <https://doi.org/10.1021/acsami.9b17241>.
- [24] L.J. van der Pauw, A method of measuring the resistivity and Hall coefficient of lamellae of arbitrary shape, *Philips Tech. Rev.* 20 (1959) 220–224.
- [25] P.S.C. Schulze, A.J. Bett, M. Bivour, P. Caprioglio, F.M. Gerspacher, Ö.Ş. Kabaklı, A. Richter, M. Stoltzer, Q. Zhang, D. Neher, M. Hermle, H. Hillebrecht, S. W. Glunz, J.C. Goldschmidt, 25.1% high-efficient monolithic perovskite silicon tandem solar cell with a high band gap perovskite absorber, *Sol. RRL* 4 (2020), 2000152, <https://doi.org/10.1002/solr.202000152>.
- [26] M. Meusel, R. Adelhelm, F. Dimroth, A.W. Bett, W. Warta, Spectral mismatch correction and spectrometric characterization of monolithic III-V multi-junction solar cells, *Prog. Photovoltaics Res. Appl.* 10 (2002) 243–255, <https://doi.org/10.1002/ppp.407>.
- [27] J. Ziegler, L. Xia, R. Zejnelovic, D. Borchert, Changes in contact resistance of different metals to magnetron sputtered ito while annealing, in: *Proceedings of the 5th World Conference on Photovoltaic Energy Conversion, Valencia, Spain, 2010*, pp. 1740–1743.
- [28] C. Luderer, L. Tutsch, C. Messmer, M. Hermle, M. Bivour, Influence of TCO and a-Si:H doping on SHJ contact resistivity, *IEEE J. Photovoltaics* 11 (2021) 329–336, <https://doi.org/10.1109/JPHOTOV.2021.3052106>.
- [29] K. Sveinbjörnsson, B. Li, S. Mariotti, E. Jarzemowski, L. Kegelmann, A. Wirtz, F. Frühauf, A. Wehrauch, R. Niemann, L. Korte, F. Fertig, J.W. Müller, S. Albrecht, Monolithic perovskite/silicon tandem solar cell with 28.7% efficiency using industrial silicon bottom cells, *ACS Energy Lett.* 7 (2022) 2654–2656, <https://doi.org/10.1021/acsenergylett.2c01358>.
- [30] P. Tockhorn, J. Sutter, A. Cruz, P. Wagner, K. Jäger, D. Yoo, F. Lang, M. Grischek, B. Li, J. Li, O. Shargaieva, E. Unger, A. Al-Ashouri, E. Köhnen, M. Stoltzer, D. Neher, R. Schlattmann, B. Rech, B. Stannowski, S. Albrecht, C. Becker, Nano-optical designs for high-efficiency monolithic perovskite-silicon tandem solar cells. Preprint, *Nat. Nanotechnol.* (2022), <https://doi.org/10.1038/s41565-022-01228-8> to be published.
- [31] E. Aydin, T.G. Allen, M. de Bastiani, L. Xu, J. Ávila, M. Salvador, E. van Kerschaver, S. de Wolf, Interplay between temperature and bandgap energies on the outdoor performance of perovskite/silicon tandem solar cells, *Nat. Energy* 5 (2020) 851–859, <https://doi.org/10.1038/s41560-020-00687-4>.
- [32] A.J. Bett, D. Chojniak, M. Schachtner, S.K. Reichmuth, Ö.Ş. Kabaklı, P.S.C. Schulze, O. Fischer, F. Schindler, J. Hohl-Ebinger, G. Siefert, M.C. Schubert, Spectrometric characterization of monolithic perovskite/silicon tandem solar cells, *Sol. RRL* sol. (2022), 202200948, <https://doi.org/10.1002/solr.202200948>.
- [33] J. Metzendorf, Calibration of solar cells. 1. The differential spectral responsivity method, *Appl. Opt.* 26 (1987) 1701–1708, <https://doi.org/10.1364/AO.26.001701>.
- [34] M. Saliba, L. Etgar, Current density mismatch in perovskite solar cells, *ACS Energy Lett.* 5 (2020) 2886–2888, <https://doi.org/10.1021/acsenergylett.0c01642>.
- [35] M. Mundus, B. Venkataramanachar, R. Gehlhaar, M. Kohlstädt, B. Niesen, W. Qiu, J.P. Herterich, F. Sahli, M. Bräuninger, J. Werner, J. Hohl-Ebinger, G. Uytterhoeven, U. Würfel, C. Ballif, M.C. Schubert, W. Warta, S.W. Glunz, Spectrally resolved nonlinearity and temperature dependence of perovskite solar cells, *Sol. Energy Mater. Sol. Cell.* 172 (2017) 66–73, <https://doi.org/10.1016/j.solmat.2017.07.013>.

- [36] M. Meusel, C. Baur, G. Létay, A.W. Bett, W. Warta, E. Fernandez, Spectral response measurements of monolithic GaInP/Ga(In)As/Ge triple-junction solar cells: measurement artifacts and their explanation, *Prog. Photovoltaics Res. Appl.* 11 (2003) 499–514, <https://doi.org/10.1002/ppp.514>.
- [37] S. Lange, S. Hensel, A. Hähnel, V. Naumann, T. Urban, M. Müller, C. Hagendorf, Contact and bulk resistivity screening for advanced crystalline silicon solar cell concepts by an economical and reliable transfer length measurement method based on laser micro-patterning, *Phys. Status Solidi* 218 (2021), 2000520, <https://doi.org/10.1002/pssa.202000520>.
- [38] D. Pysch, A. Mette, S.W. Glunz, A review and comparison of different methods to determine the series resistance of solar cells, *Photovoltaics, Sol. Energy Mater. Technol.* 91 (2007) 1698–1706, <https://doi.org/10.1016/j.solmat.2007.05.026>.
- [39] M. Wolf, H. Rauschenbach, Series resistance effects on solar cell measurements, *Adv. Energy Convers.* 3 (1963) 455–479, [https://doi.org/10.1016/0365-1789\(63\)90063-8](https://doi.org/10.1016/0365-1789(63)90063-8).
- [40] M. Stolterfoht, M. Grischek, P. Caprioglio, C.M. Wolff, E. Gutierrez-Partida, F. Peña-Camargo, D. Rothhardt, S. Zhang, M. Raoufi, J. Wolansky, M. Abdi-Jalebi, S.D. Stranks, S. Albrecht, T. Kirchartz, D. Neher, How to quantify the efficiency potential of neat perovskite films: perovskite semiconductors with an implied efficiency exceeding 28, *Adv. Mater. (Weinheim, Ger.)* 32 (2020), e2000080, <https://doi.org/10.1002/adma.202000080>.
- [41] M. Saliba, T. Matsui, J.-Y. Seo, K. Domanski, J.-P. Correa-Baena, M.K. Nazeeruddin, S.M. Zakeeruddin, W. Tress, A. Abate, A. Hagfeldt, M. Grätzel, Cesium-containing triple cation perovskite solar cells: improved stability, reproducibility and high efficiency, *Energy Environ. Sci.* 9 (2016) 1989–1997, <https://doi.org/10.1039/C5EE03874J>.